RSC Advances

PAPER

View Article Online
View Journal | View Issue

Cite this: *RSC Adv.*, 2025, **15**, 11293

Adsorption of Cd^{2+} ions onto zeolites synthesized from a mixture of coal fly ash and oil shale ash in aqueous media†

Shuxia Bai,[a] Zhibing Chang,[b] Zhengchun Ren,[a] Yongqin Zhao *[c] and Laixue Pang*[d]

Received 1st February 2025
Accepted 3rd April 2025

DOI: 10.1039/d5ra00752f

rsc.li/rsc-advances

Contaminated water, especially water containing high concentrations of toxic metal ions, is frequently discharged into the environment. Thus, developing advanced adsorbents with high adsorption capacities is essential for efficient pollutant removal. In this study, X- and A-type zeolites were synthesized using industrial waste materials, specifically oil shale ash and coal fly ash. Their physicochemical properties were characterized using XRD, SEM, and nitrogen adsorption–desorption analyses. The adsorption behaviors of Cd^{2+} ions onto the synthesized zeolites from aqueous solutions were thoroughly investigated, including kinetic and isotherm analyses. The results showed that the adsorption process adhered to pseudo-second-order kinetics and followed the Langmuir isotherm model for all zeolites. Maximum adsorption capacities were reached within 60 min, with a dosage of 1 g L^{-1} and at pH 7. Among the zeolites, OSA75 demonstrated the highest Cd^{2+} adsorption capacity, reaching 236.41 mg g^{-1}, indicating that the incorporation of a small amount of coal fly ash significantly enhanced the adsorption performance. The dominant mechanism governing Cd^{2+} adsorption was identified as cation exchange.

1. Introduction

Contaminated water, particularly water containing high concentrations of toxic metal ions, is often discharged into the environment. The persistence, accumulation, and toxicity of heavy metals in wastewater necessitate the development of effective removal strategies. Among these pollutants, cadmium is particularly detrimental to aquatic ecosystems and human health, as it is classified as a carcinogen.[1] In recent years, various treatment technologies, such as chemical precipitation, flocculation, and electrochemical processes, have been proposed to mitigate the presence of heavy metals in wastewater.[2,3] However, many of these approaches are hindered by limitations such as high operational costs and suboptimal efficiency. In contrast, adsorption has gained prominence as a preferred approach for removing toxic metals, owing to its straightforward operation, cost-efficiency, and remarkable effectiveness.[4]

Various adsorbents, such as clay materials,[5–7] activated carbon,[2] and geopolymers[8,9] have been tested for Cd^{2+} uptake from wastewater.[10,11] Despite these efforts, the adsorption capacities of these materials remain insufficient for treating Cd^{2+}-contaminated wastewater. Therefore, there is an urgent need to develop advanced adsorbents with high adsorption capacity. Zeolites, in particular, have garnered significant interest as promising adsorbents, attributed to their extensive surface area and highly porous structure.[12–16]

Zeolites can be derived from a range of sources, including both natural and synthetic materials, as well as pure chemical reagents. However, natural zeolites often exhibit low adsorption capacity and are limited by their reserves.[13,17] On the other hand, synthetic zeolites are costly to produce due to the use of chemical reagents.[18] To tackle these challenges, numerous researchers have explored the synthesis of zeolites from cost-effective solid waste materials, including red mud, construction waste, coal fly ash (CFA), and oil shale ash (OSA), among others.[19,20] These waste materials share mineralogical composition and structural similarities with the precursors of natural zeolites, making them viable sources of alumina and silica for zeolite synthesis. Various techniques, such as the hydrothermal method, alkaline fusion method, alkaline fusion-hydrothermal method, and microwave-assisted method, have been employed to convert these materials into zeolites. This approach not only provides a sustainable waste utilization strategy but also offers an efficient solution for the removal of heavy metals from wastewater.[21] This approach not only reduces the need for solid waste disposal but also helps mitigate heavy metal pollution.

[a]School of Construction Machinery, Shandong Jiaotong University, 250357, Jinan, Shandong, China
[b]School of Chemical & Environmental Engineering, China University of Mining and Technology (Beijing), 100083, Beijing, China
[c]Jinan Preschool Education College, 250307, Jinan, Shandong, China. E-mail: yongqin-zhao@outlook.com
[d]School of Traffic and Civil Engineering, Shandong Jiaotong University, 250357, Jinan, Shandong, China. E-mail: lxpang@sdjtu.edu.cn

† Electronic supplementary information (ESI) available. See DOI: https://doi.org/10.1039/d5ra00752f

Several studies have investigated the potential of zeolites synthesized from CFA and OSA for heavy metal removal.[11,13,22–26] However, research on synthesizing zeolites from solid wastes with varying silicon and aluminum contents remains limited.

The high silicon content in OSA and the elevated aluminum levels in CFA offer a promising opportunity for their combined use in zeolite synthesis. This study aims to synthesize zeolites from these materials and evaluate their effectiveness in removing Cd^{2+} from aqueous solutions. The effects of pH, contact time, and initial Cd^{2+} concentration on adsorption were systematically examined. Kinetic models were employed to determine adsorption parameters, while isotherm models were applied to characterize equilibrium behavior. Additionally, the mechanisms underlying Cd^{2+} adsorption onto the synthesized zeolites were investigated. This research provides a promising approach to mitigating environmental challenges related to both solid waste disposal and heavy metal-contaminated wastewater, aligning with the "waste-for-waste" treatment concept.

2. Experimental

2.1. Materials

This study utilized CFA and OSA as the primary raw materials, sourced from an oil-shale-fired power plant in Shandong and a coal-fired station in Shanxi, China. The chemical compositions of OSA and CFA were determined using XRF, and the results are presented in Table S1.† The SiO_2/Al_2O_3 weight ratio for OSA was found to be 3.59, in contrast to 1.17 for CFA, indicating a higher silicon content in OSA and a higher aluminum content in CFA. X-ray diffraction (XRD) analysis (Fig. 1) revealed that OSA primarily contained quartz, while CFA exhibited a glassy amorphous phase, characterized by a broad peak between 15° and 30°. Scanning electron microscopy (SEM) images (Fig. 2) showed that OSA consisted mainly of dense phases with occasional glass beads, whereas CFA particles were granular with smooth surfaces.

Analytical-grade sodium hydroxide (NaOH) and cadmium chloride ($CdCl_2 \cdot 2.5H_2O$) were procured from Beijing Chemical Works. Deionized water was employed consistently as the solvent. A 1000 mg L^{-1} Cd^{2+} stock solution was prepared by accurately dissolving $CdCl_2 \cdot 2.5H_2O$ in deionized water, and working solutions were subsequently prepared by appropriate dilution. The pH levels of the working solutions were adjusted using HNO_3 and NaOH solutions at concentrations of 0.01, 0.1, and 1 mol L^{-1}.[27]

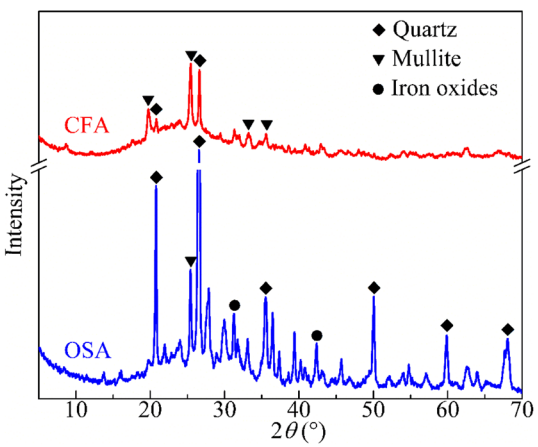

Fig. 1 XRD patterns of OSA and CFA.

2.2. Methods

2.2.1. Synthesis of zeolites. Zeolite was synthesized from OSA using the alkaline fusion hydrothermal method described in our previous study.[28] In the present work, this same procedure was employed for zeolite synthesis. Specifically, 2 g of OSA was mixed with 2.4 g of sodium hydroxide and subjected to fusion at 600 °C for 1 h. After cooling, the fused mixture was ground and added to 20 mL of deionized water. The resulting slurry was aged at room temperature with mechanical stirring for 3 h, then transferred to a Teflon-lined autoclave for crystallization at 80 °C for 12 h under static conditions. Following crystallization, the mixture was filtered, and the solid product was washed with deionized water until the pH neared 7. Finally, the product was dried at 105 °C for 2 h. The resulting zeolite, designated as OSA100, was used as the adsorbent.

Other zeolites were synthesized following the same procedure. In addition to the reference zeolite (OSA100), blended zeolites were also produced, in which OSA was partially replaced by 25%, 50%, 75%, and 100% CFA, resulting in the zeolites labeled as OSA75, OSA50, OSA25, and CFA100, respectively.

2.2.2. Adsorption experiments. Adsorption experiments were performed by introducing 0.05 g of zeolite into 50 mL of Cd^{2+} aqueous solution in uniform beakers at 30 °C. The influence of pH on adsorption capacity was assessed across a pH range of 3 to 9. Kinetic studies were conducted at intervals of 5, 10, 20, 40, 60, 80, 100, 120, and 150 min. Adsorption isotherms were determined using various initial concentrations of Cd^{2+} aqueous solutions (20, 40, 80, 100, 120, 150, 180, 200, 250, 300, 400, and 500 mg L^{-1}). The solutions were agitated at 150 rpm using a shaker, and following each experiment, the mixtures were filtered through 45 μm membranes. The concentration of residual Cd^{2+} in the filtrates was analyzed using an Inductively Coupled Plasma Emission Spectrometer (ICP). Calculations of adsorption capacity (q_e) and uptake efficiency (E%) are given in ref. 29.

2.2.3. Characterization and analysis. The chemical composition of the raw materials was determined using XRF with an Empyrean instrument. Mineralogical analysis was conducted through XRD employing a Rigaku instrument, utilizing Ni-filtered Cu Kα radiation (λ = 0.15418 nm). XRD patterns were recorded over a 2θ range of 2.5° to 70° at a scan rate of 4°·min^{-1}, and the data were processed using JADE software with the ICSD minerals database. Particle morphology was examined using SEM (ZEISS EVO18). The surface area and other surface properties of the synthesized zeolites were determined with a Micromeritics ASAP 2020 analyzer, after degassing at 300 °C for 12 h. The residual Cd^{2+} concentration in the solutions was quantified using inductively coupled plasma spectroscopy (PerkinElmer 8300).[27]

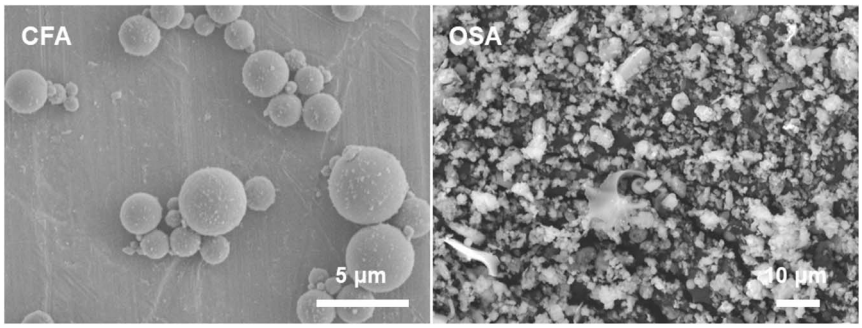

Fig. 2 SEM images of CFA and OSA.

3. Results and discussion

3.1. Characteristics of adsorbents

Fig. 3 presents the XRD patterns of the synthesized zeolites (OSA100, OSA75, OSA50, OSA25, and CFA100). The XRD pattern of OSA100 corresponds to X zeolite, which aligns closely with PDF#12-0246 ($Na_2Al_2Si_{2.4}O_{8.8}\cdot 6.7H_2O$). Similar diffraction patterns were observed for OSA75 and OSA50 (Fig. 3). In contrast, the XRD profiles of CFA100 and OSA25 closely match those of Na-A zeolite (PDF#38-0241, $Na_2Al_2Si_{1.85}O_{7.7}\cdot 5.1H_2O$). Furthermore, the synthetic zeolites exhibited well-defined crystallinity, as evidenced by the sharp and intense diffraction peaks. The Si/Al ratio of precursor materials plays a crucial role in determining the specific types of zeolites formed during hydrothermal synthesis. As the Si/Al ratio increases, the aluminum content in the synthesis system decreases, promoting the formation of X-type zeolite. Conversely, a lower Si/Al ratio creates conditions more favorable for the formation of A-type zeolite.[30,31] Consequently, when synthesizing composite zeolites by blending oil shale ash and coal fly ash, an increase in the proportion of coal fly ash reduces the overall Si/Al ratio of the raw materials. This gradual decrease shifts the synthesis conditions from favoring X-type zeolite formation to those more conducive to A-type zeolite formation. In this study, the higher aluminum content in CFA compared to OSA led to the formation of Na–A zeolite when the CFA content exceeded 50%, rather than Na–X zeolite.

Fig. 4 presents the N_2 adsorption–desorption isotherms of the synthesized zeolites, displaying type IV profiles accompanied by H3 hysteresis loops, indicative of mesoporous structures.[32] The summarized specific surface areas and pore properties of the zeolites are presented in Table 1. The BET surface area (S_{BET}) values, as listed, decrease in the following order: OSA75 > OSA100 > OSA50 > OSA25 > CFA100. Additionally, both micropores (<2 nm) and mesopores (2–50 nm) were identified in the zeolite samples. However, significant differences were observed in the micropore-to-mesopore volume ratio and the average pore diameter among the various zeolites. The ratio of mesopore volume was higher in X-type zeolite (OSA100, OSA75 and OSA50), whereas the ratio of micropore volume was higher in A-type zeolite (OSA25 and CFA100). Furthermore, the pore size of X zeolite (OSA100, OSA75 and OSA50) were larger than that of A zeolite (OSA25 and CFA100). The variation in the specific surface area of oil shale ash/coal fly ash composite zeolites is primarily attributed to differences in pore type and pore volume. Compared to A-type zeolite, X-type zeolite has a higher density of micropores, leading to a larger pore volume and, consequently, a greater specific surface area. The differences in pore size within these composite zeolites are

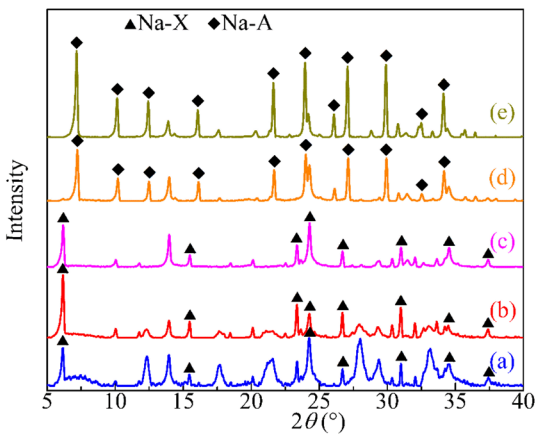

Fig. 3 XRD patterns of OSA100 (a), OSA75 (b), OSA50 (c), OSA25 (d) and CFA100 (e).

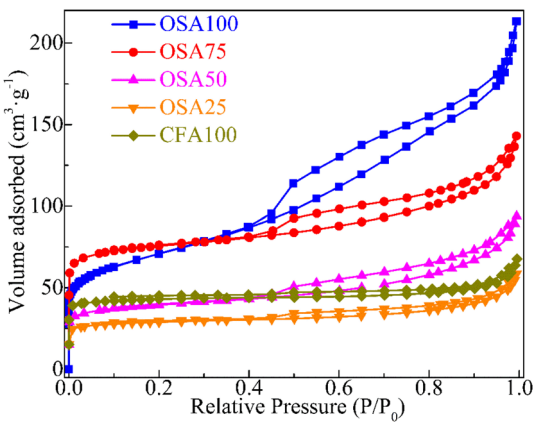

Fig. 4 N_2 adsorption–desorption isotherms of OSA100, OSA75, OSA50, OSA25 and CFA100.

Table 1 Surface characteristics of OSA100, OSA75, OSA50, OSA25 and CFA100

Samples	S_{BET} ($m^2\ g^{-1}$)	Micropore volume ($cm^3\ g^{-1}$)	Mesopore volume ($cm^3\ g^{-1}$)	Pore volume ($cm^3\ g^{-1}$)	Average pore diameter (nm)
OSA100	252.22	0.109	0.110	0.229	2.914
OSA75	288.55	0.086	0.132	0.221	3.068
OSA50	215.89	0.038	0.104	0.145	3.975
OSA25	199.04	0.073	0.033	0.111	2.330
CFA100	170.83	0.055	0.031	0.104	2.444

influenced not only by the type of pores but also by the structural characteristics of the zeolite framework. A-type zeolite belongs to the cubic crystal system, where SOD cages are arranged in a simple cubic configuration. This structure forms a three-dimensional 8-membered ring pore system with a pore diameter of 0.41 nm. In contrast, X-type zeolite falls under the hexagonal crystal system, characterized by a larger pore volume and a three-dimensional 12-membered ring pore system with a pore diameter of 0.72 nm. As a result, X-type zeolite generally exhibits a larger specific surface area, higher pore volume, and greater average pore size, whereas A-type zeolite possesses a lower specific surface area, smaller pore volume, and reduced average pore size.

3.2. Adsorption tests

3.2.1. Effect of solution pH. Fig. 5 illustrates the effect of solution pH on Cd^{2+} removal by the synthesized zeolites, with uptake efficiency plotted against pH. The results highlight the critical role of pH in Cd^{2+} adsorption. Uptake efficiency increased with rising pH, stabilizing as pH ranged from 3 to 9. Additionally, the Cd^{2+} uptake efficiency of the zeolites (OSA50, OSA25, and CFA100) increased rapidly and approached that of OSA75 when the pH exceeded 7. At lower pH values, adsorption capacity was reduced, likely due to competitive adsorption by H^+ ions. As pH increased, the efficiency of Cd^{2+} removal improved, which can be attributed to two main factors: first, the competitive adsorption of H^+ ions progressively diminished and ultimately ceased, and second, the precipitation of Cd^{2+} occurred at pH values above 7.[33] Consequently, a pH of 7 was selected for subsequent experiments, as it optimized adsorption capacity while avoiding precipitation.

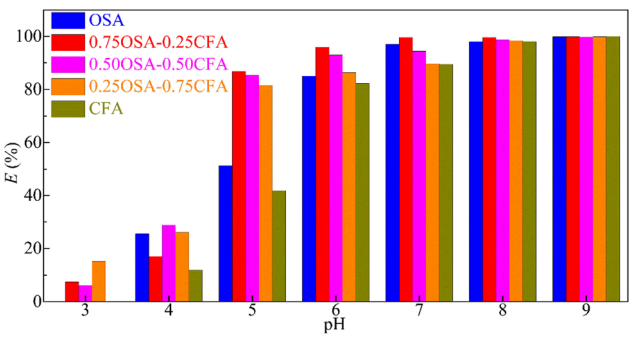

Fig. 5 Influence of solution pH on Cd^{2+} adsorption by zeolites (m = 1 g L^{-1}, t = 120 min, C_0 = 100 mg L^{-1}, T = 30 °C).

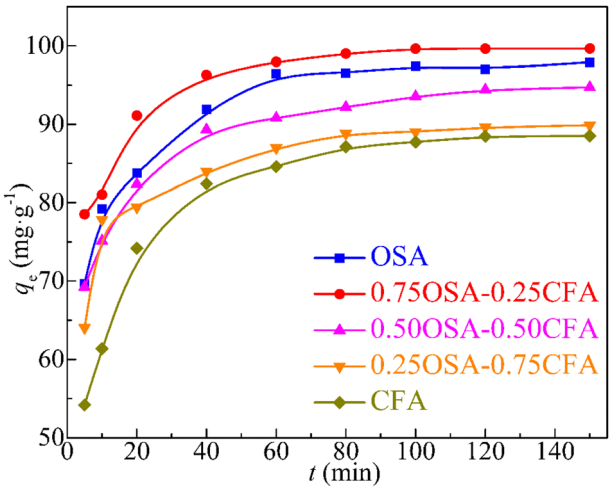

Fig. 6 Impact of contact time on Cd^{2+} adsorption onto zeolites (m = 1 g L^{-1}, pH 7, C_0 = 100 mg L^{-1}, T = 30 °C).

3.2.2. Adsorption kinetics. Fig. 6 demonstrates the effect of contact time on Cd^{2+} adsorption by the synthesized zeolites. The adsorption capacity increased steadily within the 5-150 min timeframe. The initial adsorption rate was rapid, gradually slowing as the system neared equilibrium, where the Cd^{2+} adsorbed by the zeolites balanced with the residual Cd^{2+} concentration in the solution. As shown in Fig. 6, no significant variation in Cd^{2+} removal was observed for any of the zeolites after 60 min.

To investigate the adsorption kinetics of Cd^{2+} on synthetic zeolites, three models were evaluated: pseudo-first-order, pseudo-second-order, and intraparticle diffusion models.[10,34,35] The relevant parameters and correlation coefficients are provided in Table S2.† Among these, the pseudo-second-order model demonstrated the best agreement with the experimental data, as illustrated in Fig. 7. For all synthetic zeolites, the correlation coefficients (R^2) for the pseudo-second-order model were greater than 0.999, substantially outperforming those of the other models. Furthermore, the experimentally measured adsorption capacities ($q_{e,exp}$) closely matched the theoretical values ($q_{e,cal}$) predicted by this model. These findings confirm that the adsorption process of Cd^{2+} onto synthetic zeolites is most accurately described by the pseudo-second-order model, indicating a mechanism predominantly governed by chemisorption.[36]

3.2.3. Adsorption isotherm. Fig. 8 illustrates the influence of the initial Cd^{2+} concentration on its adsorption behavior by

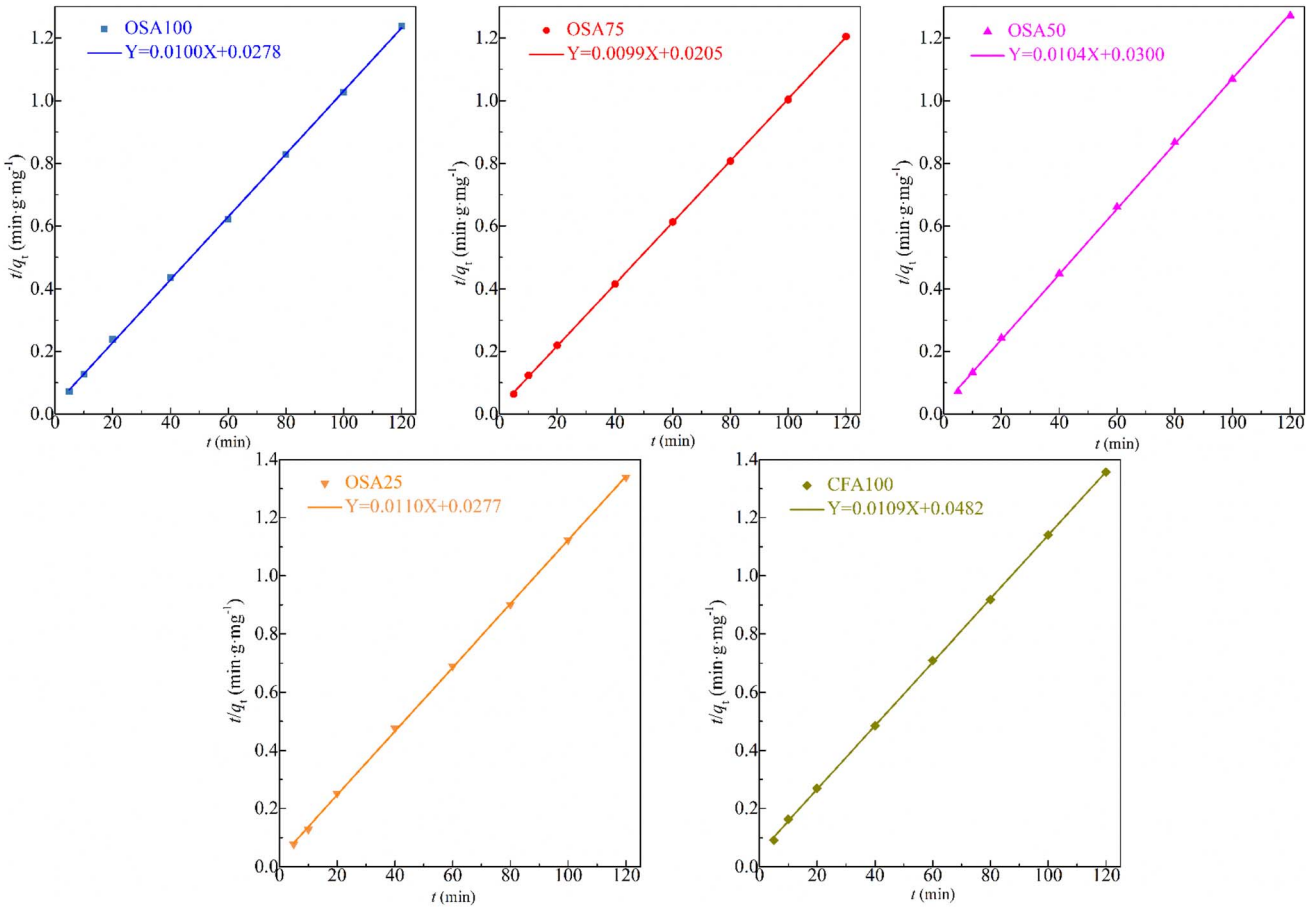

Fig. 7 Pseudo-second-order kinetic model for Cd^{2+} adsorption onto zeolites.

synthetic zeolites. With an increase in the initial concentration from 20 to 500 mg L^{-1}, the equilibrium adsorption capacities exhibited a marked enhancement. Among the zeolites, OSA75 exhibited the highest adsorption capacity, attributable to its larger BET surface area and higher availability of exchangeable cations. These factors significantly enhanced its Cd^{2+} uptake efficiency.[37]

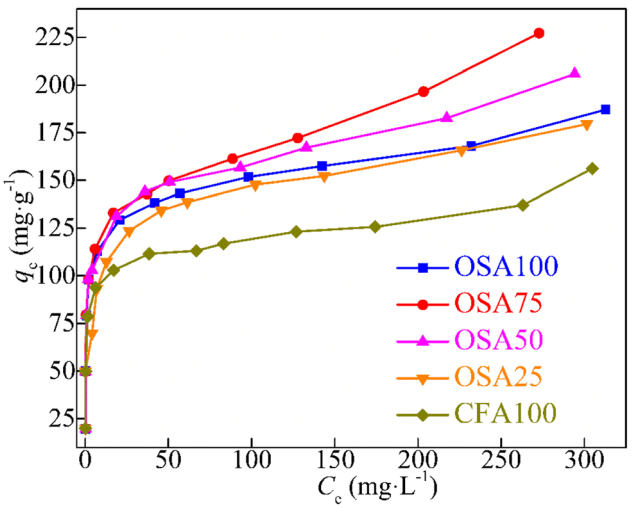

Fig. 8 Influence of initial Cd^{2+} concentration on adsorption behavior of zeolites (m = 1 g L^{-1}, pH 7, t = 60 min, T = 30 °C).

Adsorption isotherms are crucial for understanding adsorption mechanisms, as they reveal the interactions between adsorbate molecules and the active sites of the adsorbent surface. In this study, the adsorption behavior of Cd^{2+} on synthetic zeolites was assessed using the Langmuir, Freundlich, and Dubinin–Radushkevich (D–R) models.[38–40] Fig. 9 presents the Langmuir adsorption isotherm curves for Cd^{2+} on synthetic zeolites along with their linear fits. The corresponding isotherm parameters and correlation coefficients are summarized in Table S3.† The Langmuir model showed the highest correlation coefficients (R^2) for all zeolites, followed by the Freundlich and D–R models, indicating that the Cd^{2+} adsorption is most accurately described by the Langmuir isotherm. This suggests that adsorption occurs in a monolayer on adsorbents with a uniform surface energy distribution. According to the Langmuir model, the maximum Cd^{2+} adsorption capacities ranked as follows: OSA75 > OSA50 > OSA100 > OSA25 > CFA100, aligning closely with experimental data in Table S3.† The highest monolayer adsorption capacity was found for OSA75 at 236.41 mg g^{-1}, followed by 211.86 mg g^{-1} for OSA50. These results underscore the superior adsorption performance of OSA75, which cannot

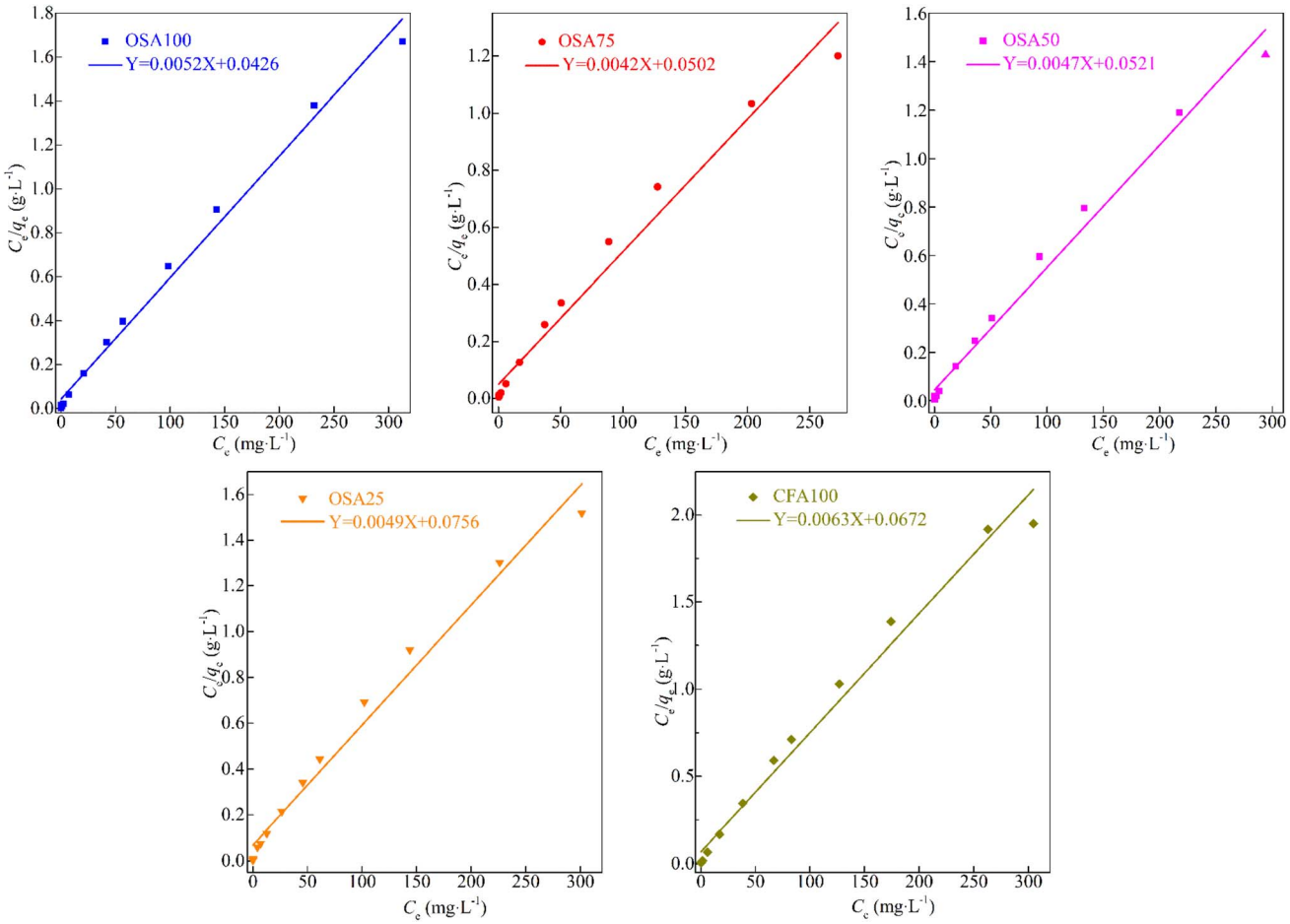

Fig. 9 Langmuir isotherm model describing Cd^{2+} adsorption onto zeolites.

be replicated by the individual raw materials. This enhanced performance can be attributed to the incorporation of a small amount of CFA, which improved the crystallinity and pore structure of the synthesized zeolite, thereby increasing its surface area and the number of exchangeable cations available for adsorption.

To evaluate the adsorption efficiency of zeolites for Cd^{2+} removal from aqueous systems, their maximum adsorption capacities were compared with those of other reported materials, as summarized in Table 2. It is evident from the data that the zeolites synthesized in this study exhibit significantly higher adsorption capacities than other adsorbents. This finding highlights the superior performance of zeolites derived from a mixture of coal fly ash and oil shale ash, making them a promising candidate for the treatment of cadmium-contaminated wastewater.

3.3. Adsorption mechanisms

The results indicate that Cd^{2+} uptake was primarily governed by ion-exchange processes on the synthetic zeolites, as supported by both the adsorption kinetics and isotherms. Despite the identical adsorption mechanism, significant variations in the adsorption capacities of the synthetic zeolites were observed. This suggests that the maximum Cd^{2+} adsorption capacity was not solely determined by specific surface area and exchangeable cations, but also influenced by additional factors, such as the structural characteristics of the zeolites. Metal ions in aqueous solutions typically exist in a hydrated form, with Cd^{2+} possessing an ionic radius of 0.97 Å and a hydrated ionic radius of 4.29 Å. When comparing the crystal radii of X-type zeolite (7.4 Å) and A-type zeolite (4.5 Å) channels, it becomes evident that both hydrated and unhydrated Cd^{2+} ions can easily traverse the channels of X-type zeolite. In contrast, the hydrated Cd^{2+} ions are similar in size to the A-type zeolite channels, which may

Table 2 Adsorption results of Cd^{2+} onto different adsorbents

Adsorption materials	Adsorption capacity (mg g^{-1})
Iranian natural zeolite	4.01 (ref. 12)
Activated carbon	111.78 (ref. 2)
Modification of nano-clays	94.6 (ref. 5)
Magnetic nano-zeolite	159.39 (ref. 17)
OSA100	187.18 (this study)
OSA75	227.24 (this study)
OSA50	205.87 (this study)
OSA25	179.54 (this study)
CFA100	156.21 (this study)

hinder their exchange unless some of the hydration water is removed. Consequently, OSA75 exhibited the highest adsorption capacity, whereas CFA100 displayed the lowest.

4. Conclusions

The X- and A-type zeolites were synthesized by recycling industrial solid wastes, specifically OSA and CFA, through the alkaline fusion hydrothermal method. These zeolites exhibited significant adsorption affinity for Cd^{2+}. Maximum adsorption capacities for all zeolites were achieved within 60 min at a concentration of 1 g L^{-1} and pH 7. The adsorption kinetics of Cd^{2+} were most accurately described by the pseudo-second-order model. Additionally, adsorption isotherm analysis revealed that the Langmuir isotherm model provided the best fit, indicating monolayer adsorption behavior. Among the zeolites investigated, OSA75 exhibited the highest Cd^{2+} adsorption capacity, reaching 236.41 mg g^{-1}, with adsorption capacities following the order: OSA75 > OSA50 > OSA100 > OSA25 > CFA100. These results suggest that incorporating a small proportion of CFA during zeolite synthesis enhanced adsorption performance. The Cd^{2+} uptake by the synthetic zeolites was primarily attributed to ion-exchange processes, suggesting a chemical adsorption mechanism. Additionally, the structural and surface properties of the zeolites significantly contributed to their enhanced adsorption capacities. These findings suggest that synthesizing zeolites from a combination of solid wastes offers a promising approach for wastewater treatment applications.

Data availability

The data supporting this article have been included as part of the ESI.†

Author contributions

Shuxia Bai: writing – original draft, visualization, validation, methodology, investigation, formal analysis, data curation, conceptualization. Zhibing Chang: writing – review & editing, supervision, validation, methodology. Zhengchun Ren: visualization, investigation, data curation. Yongqin Zhao: visualization, validation, methodology, investigation, formal analysis, data curation, conceptualization, supervision. Laixue Pang: writing – review & editing, validation, methodology, funding acquisition.

Conflicts of interest

The authors have no conflicts of interest to declare.

Acknowledgements

The authors are grateful to the financial support of the Natural Science Foundation of Shandong Province (ZR2020ME231).

References

1 S. Iyer, S. M. Deshmukh and R. W. Tapre, Review on removal of heavy metals from industrial effluents by adsorption, *Rev. Inorg. Chem.*, 2024, **22**, 1–18.
2 S. Pap, T. Šolević Knudsen, J. Radonić, S. Maletić, S. M. Igić, *et al.*, Utilization of fruit processing industry waste as green activated carbon for the treatment of heavy metals and chlorophenols contaminated water, *J. Cleaner Prod.*, 2017, **162**, 958–972.
3 S. Taihong, Y. Di, Y. Huizhu, Y. Jinpeng and C. Qiankun, Preparation of chitosan crosslinked modified silicon material and its adsorption capability for chromium(VI), *Appl. Clay Sci.*, 2017, **142**, 100–108.
4 F. Fu and Q. Wang, Removal of heavy metal ions from wastewaters: a review, *J. Environ. Manage.*, 2011, **92**(3), 407–418.
5 A. Naderi, M. A. Delavar, Y. Ghorbani, B. Kaboudin and M. Hosseini, Modification of nano-clays with ionic liquids for the removal of Cd (II) ion from aqueous phase, *Appl. Clay Sci.*, 2018, **158**, 236–245.
6 P. W. Chen, M. N. Hsiao, L. W. Xiao, *et al.*, Adsorption behavior of heavy metals onto microplastics derived from conventional and biodegradable commercial plastic products, *Sci. Total Environ.*, 2024, **951**, 175537.
7 H. S. Ibrahim, T. S. Jamil and E. Z. Hegazy, Application of zeolite prepared from Egyptian kaolin for the removal of heavy metals: II. Isotherm models, *J. Hazard. Mater.*, 2010, **182**(1–3), 842–847.
8 A. Sudagar, S. Andrejkovičová, C. Patinha, A. Velosa, A. McAdam, E. F. da Silva, *et al.*, A novel study on the influence of cork waste residue on metakaolin-zeolite based geopolymers, *Appl. Clay Sci.*, 2018, **152**, 196–210.
9 S. Andrejkovičová, A. Sudagar, J. Rocha, C. Patinha, W. Hajjaji, E. F. da Silva, *et al.*, The effect of natural zeolite on microstructure, mechanical and heavy metals adsorption properties of metakaolin based geopolymers, *Appl. Clay Sci.*, 2016, **126**, 141–152.
10 S. Dash, H. Chaudhuri, R. Gupta, U. G. Nair and A. Sarkar, Fabrication and Application of Low-Cost Thiol Functionalized Coal Fly Ash for Selective Adsorption of Heavy Toxic Metal Ions from Water, *Ind. Eng. Chem. Res.*, 2017, **56**(6), 1461–1470.
11 M. Visa, Synthesis and characterization of new zeolite materials obtained from fly ash for heavy metals removal in advanced wastewater treatment, *Powder Technol.*, 2016, **294**, 338–347.
12 H. Merrikhpour and M. Jalali, Comparative and competitive adsorption of cadmium, copper, nickel, and lead ions by Iranian natural zeolite, *Clean Technol. Environ. Policy*, 2012, **15**(2), 303–316.
13 S. Bai, M. Chu, L. Zhou, Z. Chang, C. Zhang and B. Liu, Removal of heavy metals from aqueous solutions by X-type zeolite prepared from combination of oil shale ash and coal fly ash, *Energy Sources, Part A Recovery, Util. Environ. Eff.*, 2022, **44**(2), 5113–5123.

14 M. Z. Ahmed, Q. S. Ali, A. M. Essam, A. W. Mahmoud, K. S. Moaaz, *et al.*, Adsorption characteristics of Na-A zeolites synthesized from Egyptian kaolinite for manganese in aqueous solutions response surface modeling and optimization, *Appl. Clay Sci.*, 2017, **140**, 17–24.

15 M. R. Zaeri and F. Esmaeilzadeh, Performance Evaluation of Static and Dynamic CO_2 Adsorption from Synthetic Gas Condensates Using Zinc Oxide, Silicon Dioxide and Zeolite 13X, *Korean J. Chem. Eng.*, 2024, **41**(3), 879–892.

16 T. Sirinakorn, K. Imwiset, S. Bureekaew and M. Ogawa, Inorganic modification of layered silicates toward functional inorganic-inorganic hybrids, *Appl. Clay Sci.*, 2018, **153**, 187–197.

17 H. A. Shamkhi, M. J. Abdulhasan, S. A. Raheem, H. A. M. Al-Zubaidi and A. S. K. Janbi, Optimization of heavy metals removal from wastewater by magnetic nano-zeolite using response surface methodology, *Desalin. Water Treat.*, 2023, **306**, 3–74.

18 X. D. Liu, Y. P. W, X. M. Cui, Y. He and J. Mao, Influence of synthesis parameters on NaA zeolite crystals, *Powder Technol.*, 2013, **243**, 184–193.

19 W. M. Xie, F. P. Zhou, X. L. Bi, D. D. Chen, J. Li, S. Y. Sun, J. Y. Liu and X. Q. Chen, Accelerated crystallization of magnetic 4A-zeolite synthesized from red mud for application in removal of mixed heavy metal ions, *J. Hazard. Mater.*, 2018, **358**, 441–449.

20 Q. L. Qiu, X. G. Jiang, G. J. Lv, Z. L. Chen, S. Y. Lu, M. J. Ni, J. H. Yan and X. B. Deng, Adsorption of heavymetal ions using zeolite materials ofmunicipal solid waste incineration fly ash modified by microwave-assisted hydrothermal treatment, *Powder Technol.*, 2018, **335**, 156–163.

21 J. L. X. Hong, T. Maneerung, S. N. Koh, S. Kawi and C.-H. Wang, Conversion of Coal Fly Ash into Zeolite Materials: Synthesis and Characterizations, Process Design, and Its Cost-Benefit Analysis, *Ind. Eng. Chem. Res.*, 2017, **56**(40), 11565–11574.

22 A. E. Burakov, E. V. Galunin, I. V. Burakova, A. E. Kucherova, S. Agarwal, A. G. Tkachev, *et al.*, Adsorption of heavy metals on conventional and nanostructured materials for wastewater treatment purposes: a review, *Ecotoxicol. Environ. Saf.*, 2018, **148**, 702–712.

23 W. Bao, L. Liu, H. Zou, S. Gan, X. Xu, G. Ji, *et al.*, Removal of Cu^{2+} from Aqueous Solutions Using Na-A Zeolite from Oil Shale Ash, *Chin. J. Chem. Eng.*, 2013, **21**(9), 974–982.

24 X. H. Xu, K. G. Chen, Y. Dai, X. P. Xing and L. Sun, Synthesis of Zeolite A-X from Coal Fly Ash via Ultrasonic-Alkali Fusion Hydrothermal Method for the Efficient Removal of Cr (VI) From Wastewater, *Water, Air, Soil Pollut.*, 2025, **236**(2), 137.

25 R. Shawabkeh, A. Al-Harahsheh, M. Hami and A. Khlaifat, Conversion of oil shale ash into zeolite for cadmium and lead removal from wastewater, *Fuel*, 2004, **83**(7–8), 981–985.

26 H. Zhang, J. Wang, B. Zhang, Q. Liu, S. Li, H. Yan, *et al.*, Synthesis of a hydrotalcite-like compound from oil shale ash and its application in uranium removal, *Colloids Surf., A*, 2014, **444**, 129–137.

27 S. Bai, M. Chu, L. Zhou, Z. Chang, C. Zhang, H. Guo, *et al.*, Modified oil shale ash and oil shale ash zeolite for the removal of Cd^{2+} ion from aqueous solutions, *Environ. Technol.*, 2019, **40**(11), 1485–1493.

28 S.-x. Bai, L.-m. Zhou, Z.-b. Chang, C. Zhang and M. Chu, Synthesis of Na-X zeolite from Longkou oil shale ash by alkaline fusion hydrothermal method, *Carbon Resour. Convers.*, 2018, **1**, 245–250.

29 S. Ghorai, A. Sinhamahpatra, A. Sarkar, A. B. Panda and S. Pal, Novel biodegradable nanocomposite based on XG-g-PAM/SiO_2: application of an efficient adsorbent for Pb^{2+} ions from aqueous solution, *Bioresour. Technol.*, 2012, **119**, 181–190.

30 L. C. Hsiao and H. S. Wei, A General Method for the Conversion of Fly Ash into Zeolites as Ion Exchangers for Cesium, *Ind. Eng. Res.*, 1998, **37**, 71–78.

31 N. Shigemoto and H. Hayashi, Selective formation of Na-X zeolite from coal fly ash by fusion with sodium hydroxide prior to hydrothermal reaction, *J. Mater. Sci.*, 1993, **28**, 4781–4786.

32 V. B. Yadav, R. Gadi and S. Kalra, Synthesis and characterization of novel nanocomposite by using kaolinite and carbon nanotubes, *Appl. Clay Sci.*, 2018, **155**, 30–36.

33 J. He, Y. Li, C. Wang, K. Zhang, D. Lin, L. Kong, *et al.*, Rapid adsorption of Pb, Cu and Cd from aqueous solutions by β-cyclodextrin polymers, *Appl. Clay Sci.*, 2017, **426**, 29–39.

34 F. J. López, S. Sugita, M. Tagaya and T. Kobayashi, Metakaolin-Based Geopolymers for Targeted Adsorbents to Heavy Metal Ion Separation, *J. Mater. Sci. Chem. Eng.*, 2014, **02**(07), 16–27.

35 Q. Zhen, Z. Xintong, H. Hui and Z. Qiuzhuo, Properties of Spartina alterniflora Loisel. derived-biochar and its effect on cadmium adsorption, *J. Agro-Environ. Sci.*, 2018, **37**(1), 172–178.

36 Y. Y. Wang, Y. X. Liu, H. H. Lu, R. Q. Yang and S. M. Yang, Competitive adsorption of Pb(II), Cu(II), and Zn(II) ions onto hydroxyapatite-biochar nanocomposite in aqueous solutions, *J. Solid State Chem.*, 2018, **261**, 53–61.

37 A. Alshameri, H. He, J. Zhu, Y. Xi, R. Zhu, L. Ma, *et al.*, Adsorption of ammonium by different natural clay minerals: Characterization, kinetics and adsorption isotherms, *Appl. Clay Sci.*, 2018, **159**, 83–93.

38 V. J. Inglezakis, M. M. Fyrillas and M. A. Stylianou, Two-phase homogeneous diffusion model for the fixed bed sorption of heavy metals on natural zeolites, *Microporous Mesoporous Mater.*, 2018, **266**, 164–176.

39 Y. F. Wang, S. Liu, J. Y. Pan, H. Y. Zhang, B. Y. Wang and W. F. Yan, MER Zeolite with Remarkable Pb^{2+} and Cd^{2+} Removal Capability Cost-Effectively Synthesized from Postprocessed Natural Stellerite, *Inorg. Chem.*, 2024, **64**(1), 393–403.

40 X. Chen, K. Wendell, J. Zhu, J. Li, X. Yu and Z. Zhang, Synthesis of nano-zeolite from coal fly ash and its potential for nutrient sequestration from anaerobically digested swine wastewater, *Bioresour. Technol.*, 2012, **110**, 79–85.